The influence of iodine on the Antarctic stratospheric ozone hole

Carlos A. Cuevas[a,1], Rafael P. Fernandez[b,c], Douglas E. Kinnison[d], Qinyi Li[a], Jean-François Lamarque[e], Tarek Trabelsi[f], Joseph S. Francisco[f], Susan Solomon[g], and Alfonso Saiz-Lopez[a,1]

[a]Department of Atmospheric Chemistry and Climate, Institute of Physical Chemistry Rocasolano, Spanish National Research Council, Madrid 28006, Spain; [b]Institute for Interdisciplinary Science, National Research Council, Mendoza 5501, Argentina; [c]School of Natural Sciences, National University of Cuyo, Mendoza 5501, Argentina; [d]Atmospheric Chemistry Observation and Modeling, National Center for Atmospheric Research, Boulder, CO 80305; [e]Climate and Global Dynamics Laboratory, National Center for Atmospheric Research, Boulder, CO 80305; [f]Department of Chemistry, University of Pennsylvania, Philadelphia, PA 19104; and [g]Department of Earth, Atmospheric, and Planetary Sciences, Massachusetts Institute of Technology, Cambridge, MA 02139

Edited by Mark Thiemens, Chemistry and Biochemistry, University of California San Diego, La Jolla, CA; received June 11, 2021; accepted December 14, 2021

The catalytic depletion of Antarctic stratospheric ozone is linked to anthropogenic emissions of chlorine and bromine. Despite its larger ozone-depleting efficiency, the contribution of ocean-emitted iodine to ozone hole chemistry has not been evaluated, due to the negligible iodine levels previously reported to reach the stratosphere. Based on the recently observed range (0.77 ± 0.1 parts per trillion by volume [pptv]) of stratospheric iodine injection, we use the Whole Atmosphere Community Climate Model to assess the role of iodine in the formation and recent past evolution of the Antarctic ozone hole. Our 1980–2015 simulations indicate that iodine can significantly impact the lower part of the Antarctic ozone hole, contributing, on average, 10% of the lower stratospheric ozone loss during spring (up to 4.2% of the total stratospheric column). We find that the inclusion of iodine advances the beginning and delays the closure stages of the ozone hole by 3 d to 5 d, increasing its area and mass deficit by 11% and 20%, respectively. Despite being present in much smaller amounts, and due to faster gas-phase photochemical reactivation, iodine can dominate (∼73%) the halogen-mediated lower stratospheric ozone loss during summer and early fall, when the heterogeneous reactivation of inorganic chlorine and bromine reservoirs is reduced. The stratospheric ozone destruction caused by 0.77 pptv of iodine over Antarctica is equivalent to that of 3.1 (4.6) pptv of biogenic very short-lived bromocarbons during spring (rest of sunlit period). The relative contribution of iodine to future stratospheric ozone loss is likely to increase as anthropogenic chlorine and bromine emissions decline following the Montreal Protocol.

iodine | ozone depletion | Antarctic ozone hole

The role played by chlorine atoms in the catalytic destruction of stratospheric ozone, after the photolytic dissociation of chlorofluorocarbons emitted by anthropogenic activities, was proposed by Molina and Rowland (1) in the 1970s. The decrease in the stratospheric ozone column density in early spring over Antarctica was discovered in 1985 by Farman et al. (2). Further use of satellite measurements (3) defined the region in which stratospheric ozone was highly depleted. Simultaneous ground-based measurements of stratospheric ClO, HCl, $ClONO_2$, and OClO over Antarctica during springtime in 1986 (4–6) determined the key role of active chlorine chemistry on ozone hole formation. This was confirmed by the remarkable anticorrelation in the time evolution of observed high ClO levels and the strong ozone depletion reported by aircraft observations in the lower stratosphere (LS) (7). Bromine was also identified to participate in the catalytic cycling of stratospheric ozone destruction through coupling with chlorine radicals (8, 9). Most of the stratospheric bromine comes from anthropogenic emissions of long-lived sources such as halons (10, 11), although biogenic very short-lived substances (VSLS) naturally emitted from the ocean also contribute ∼25% to the stratospheric bromine burden (11–16).

In the 1990s, Solomon et al. (17) already speculated that, if 1 pptv (parts per trillion by volume) of iodine was injected to the stratosphere, iodine chemistry could be a contributing factor in widespread ozone depletion in the LS. However, subsequent observational work estimated that the total amount of iodine entering the stratosphere was less than 0.15 pptv (18–22), which was considered to have a negligible role in stratospheric ozone photochemistry (23). Recent modeling work based on novel tropospheric profile observations of iodine oxide (IO) suggested that the levels of iodine injected to the stratosphere were more likely to be ∼0.7 pptv (24). More recently, direct measurements of IO and particulate iodine in the upper troposphere (UT) and LS, in combination with models, have indeed confirmed that 0.77 ± 0.10 pptv of total inorganic iodine (both gas and particulate phase) enters the stratosphere via tropical convective outflow (25). Even though there are still uncertainties regarding the processes controlling iodine gas-to-particle partitioning during reactive transport to the stratosphere (25), the contribution of the observed stratospheric iodine injection to ozone loss within the Antarctic ozone hole remains unknown. As most of the available iodine is thought to be of natural origin, iodine can affect stratospheric ozone in the preanthropogenic atmosphere (particularly via photolysis of OIO, reaction of IO

Significance

The role of chlorine and bromine in Antarctic stratospheric ozone depletion is well known. However, the contribution of iodine to the ozone hole chemistry has not been assessed, mainly due to the negligible amounts of iodine previously reported to enter the stratosphere. New measurements demonstrate that the injection of iodine to the lower stratosphere is higher than previously assumed. Based on these observations, our modeling work shows that iodine chemistry can enhance spring ozone loss at the lower part of the Antarctic ozone hole, and even dominate the halogen-mediated ozone loss during summer. Iodine can also alter, by several days, the timing of the seasonal formation and closure of the ozone hole.

Author contributions: C.A.C. and A.S.-L. designed research; C.A.C., R.P.F., D.E.K., T.T., J.S.F., S.S., and A.S.-L. performed research; R.P.F., D.E.K., Q.L., T.T., J.S.F., and S.S. contributed new reagents/analytic tools; C.A.C., R.P.F., D.E.K., Q.L., J.-F.L., T.T., J.S.F., S.S., and A.S.-L. analyzed data; and C.A.C., R.P.F., and A.S.-L. wrote the paper.

The authors declare no competing interest.

This article is a PNAS Direct Submission.

[1]To whom correspondence may be addressed. Email: ccuevas@iqfr.csic.es or a.saiz@csic.es.

This article contains supporting information online at http://www.pnas.org/lookup/suppl/doi:10.1073/pnas.2110864119/-/DCSupplemental.

Published February 7, 2022.

Table 1. SD-WACCM4 simulations considered in this study

Run	Time period	Iodine emissions	Biogenic bromine VSLS emissions	Particulate iodine implementation
Iodine (base simulation)	1980–2015	Yes	Yes	No
No Br VSLS	1980–2015	Yes	No	No
I_{part}	1980–2015	Yes	Yes	Yes
No iodine	1980–2015	No	Yes	No

with HO_2, or reaction of IO with natural BrO). Iodine can also deplete stratospheric ozone as chlorine and bromine increase due to anthropogenic perturbations in ClO and BrO, due to what are referred to here as interhalogen reactions (i.e., IO+ClO and IO+BrO). In this paper, we evaluate the overall effect of iodine on Antarctic stratospheric ozone and do not explicitly separate the portion affected by anthropogenic activity.

We use the specified dynamics version of the Whole Atmosphere Community Climate Model, version 4 (SD-WACCM4) (26–29), to assess the currently neglected role played by iodine chemistry in the formation and evolution of the stratospheric ozone hole between 1980 and 2015, based on the recently measured range of iodine injection to the stratosphere (24, 25). The model is updated with a state-of-the-art scheme of the atmospheric chemistry of halogens from the Earth's surface to the stratopause (30–32), reproducing the recently measured range of stratospheric iodine injection (24, 25). We find that the contribution of iodine to ozone destruction can be up to 18% at 140 hPa during the Antarctic spring in the region 90°S to 70°S, with a maximum decrease of ∼4.2% in the stratospheric ozone column. Notably, the inclusion of iodine sources and chemistry advances the initial formation and delays the closure stages of the Antarctic ozone hole seasonal cycle. Our model results also reveal that, during the austral summer and fall, iodine can prevail as the dominant (∼73%) halogen-driven ozone destruction chemistry in the Antarctic LS.

Iodine Transport to the Stratosphere and Gas-to-Particle Partitioning

Recent aircraft observations supported by a global model reported that 0.77 ± 0.10 pptv of total inorganic iodine (I_y = I+2×I_2+IO+OIO+HI+HOI+INO+INO_2+$IONO_2$+IBr+ICl+2×I_2O_2+2×I_2O_3+2×I_2O_4) are currently being injected to the stratosphere, of which ∼0.21 pptv (27%) are in the gas phase, and ∼0.56 pptv (73%) are bound to aerosols, mainly as iodate (25). The heterogeneous ultraviolet (UV) photolysis of iodate releasing reactive iodine to the gas phase has been demonstrated in laboratory studies (33–35). We have also conducted theoretical calculations to define the energy thresholds for the photofragmentation from iodate particles back to gas-phase iodine (*SI Appendix*). The potential energy surface (PES) of IO_3^- is characterized by many excited states that are stable and display minima in their PES (their minimum located below the ground state of the neutral and correlated to dissociation limits located below the first dissociation limit of the neutral) (*SI Appendix*, Fig. S1). The absorption of a photon in the visible or near-UV region (i.e., 263 < hν < 442 nm) exciting these states may lead to the production of IO_2^-+O or IO_2+O^-. Indeed, there are three triplet states that correlate to the first dissociation limit, and these states are crossed by singlet states which correlate to the IO_2+O^- dissociation limit. The resulting IO_2 is unstable to dissociation, leading to I and O_2 (36). Alternatively, IO_3^- can photodetach an electron at wavelengths shorter than 263 nm to produce neutral IO_3, which is unstable, dissociating into I and O_2. Thus, the photon energy threshold required to photolyze the iodate ion, ∼260 nm (*SI Appendix*, Fig. S1), corresponds to a wavelength range that has a rapidly increasing actinic flux intensity in the middle stratosphere (*SI Appendix*, Fig. S2). Based on these calculations and the experimental absorption spectrum of iodate (33, 34), we compute the vertical profile of the iodate photolysis rate, which shows a very large increase in its normalized photolytic efficiency (up to 10,000 times) from the lower to the upper stratosphere (*SI Appendix*, Fig. S3). These results indicate that, despite the bulk of iodine injected to the stratosphere being particulate iodate, it can undergo increasing photofragmentation and thereby release iodine back to the gas phase, as air ascends into the tropical middle to upper stratosphere, following the general stratospheric circulation. It is therefore very likely that most, if not all, of the particulate iodate transported to the stratosphere will eventually be photoactivated back to the gas phase during stratospheric transport from the tropics to the Antarctic region.

We performed a set of specified dynamics WACCM4 simulations (*Materials and Methods* and Table 1) to assess the iodine effect on Antarctic stratospheric ozone loss, and to identify the spatial, vertical, and temporal extent of these impacts. Based on

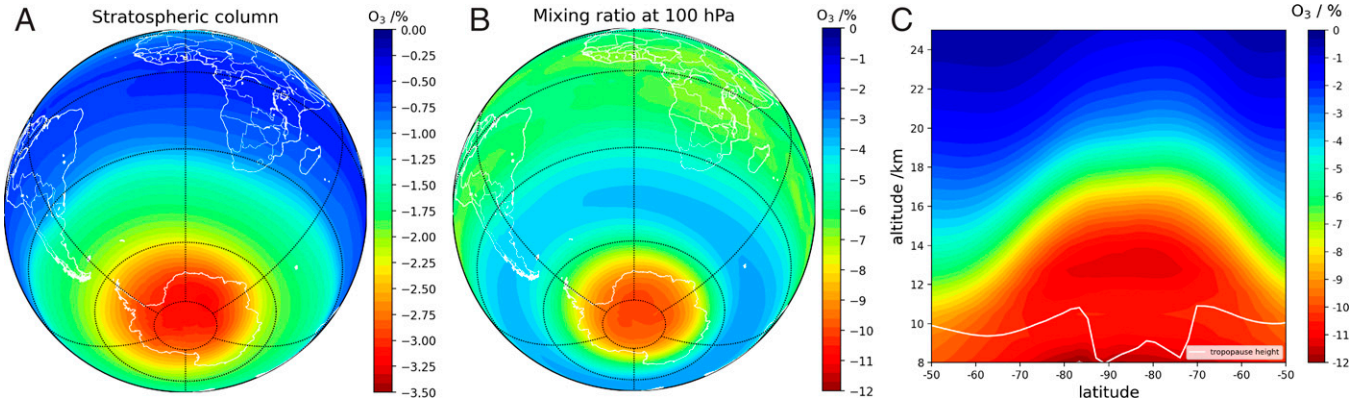

Fig. 1. The 1980–2015 September–October averaged influence of iodine chemistry on the Antarctic stratospheric ozone depletion: (*A*) percentage impact over the stratospheric vertical column; (*B*) effect at 16-km altitude (∼100 hPa); and (*C*) averaged meridional slice at 0° longitude, in which the effect of iodine chemistry can be seen spatially as a function of latitude and altitude. The relative percentage difference has been computed as ((iodine run – no iodine run)/no iodine run) × 100.

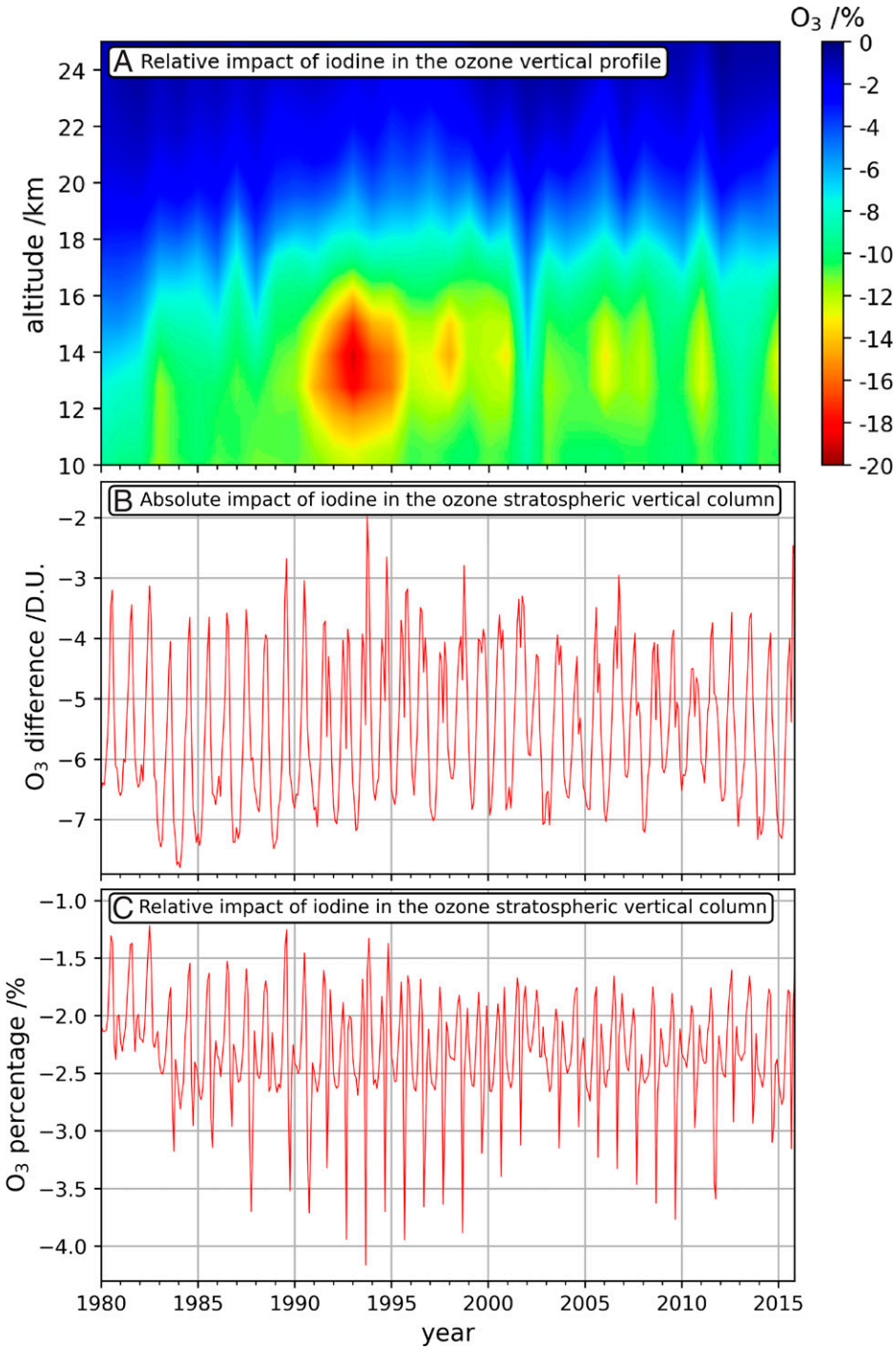

Fig. 2. (*A*) Impact of iodine in the ozone vertical profile, averaged in September and October in the 90°S to 70°S latitude region during the 1980–2015 period. (*B* and *C*) Monthly averaged iodine effect on the stratospheric ozone column in the 90°S to 70°S latitude region.

the experimental evidence and our theoretical analysis of iodate photofragmentation, our base simulation (iodine run) considers all iodine to be in gas phase. This set of simulations also includes a run with the implementation of particulate iodine (I_{part}), in which the conversion of gas-phase iodine to particulate iodine in the UT–LS is enabled. This run represents a lower limit effect of iodine on the stratospheric ozone, since a large fraction of iodine is as unreactive iodate particles, and, in addition, we do not consider ozone loss by reactive ozone uptake on iodide surfaces due to the expected low amount of iodide in stratospheric aerosols (25). The ozone differences are computed against a benchmark simulation without iodine sources and chemistry. An additional sensitivity was performed without emissions of biogenic bromine VSLS, in order to compare the relative contribution of iodine to total ozone loss with that of brominated VSLS. Hereafter, we focus on the results from the base simulation, which we consider the most likely scenario.

Antarctic Stratospheric Ozone Depletion by Iodine

We estimate that iodine chemistry accounts for a mean Antarctic spring (September and October) ozone loss of ∼3% of the

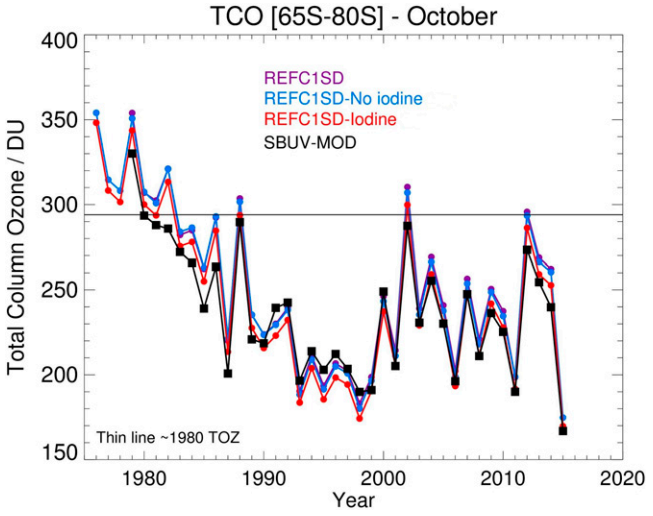

Fig. 3. October averaged evolution of the TCO in Antarctica together with SBUV-MOD satellite data. REFC1SD is the state-of-the-art WACCM simulation including MAM SAD fields employed in ref. 29. This simulation considers a surface lower boundary condition of 1.2 pptv for $CHBr_3$ and CH_2Br_2 species. The REFC1SD no iodine run includes the complete VSLS bromine scheme, but no VSLS iodine, and the REFC1SD iodine run includes both VSLS bromine and iodine. Black thin line represents the total ozone column (TOZ) in 1980.

integrated stratospheric column, averaged during the 1980–2015 simulation period in the 90°S to 70°S region (Fig. 1). Iodine causes relatively larger ozone loss at the lower part of the stratospheric ozone hole (10% in the 11- to 16-km range averaged for spring during the simulation period, and up to 18% at 14 km [approximately 140 hPa] in spring 1993 [Fig. 2]). Overall, the effect of iodine on Antarctic stratospheric ozone is mainly located in the altitude range spanning from the tropopause (~11 km) to about 16 km (Fig. 1*C*). Note that even the lower limit "I_{part}" simulation, with ~4 times less gas-phase iodine than our base case, yields a spring ozone loss of 3.5% averaged in the 90°S to 70°S region at 11- to 16-km altitude. In this case, the ozone depletion is modeled to be up to 8% in spring 1993 at 13-km altitude (*SI Appendix*, Fig. S4).

The inclusion of iodine leads to a slight improvement in the comparison of modeled total column ozone (TCO) in Antarctica with SBUV-MOD (Solar Backscatter UV instrument–Merged Ozone Dataset) satellite observations during the 1980–2015 period (Fig. 3). Note that there is a good agreement between our model run without iodine and previous state-of-the-art SD-WACCM4 model simulations (29). The simulation including iodine also slightly improves the agreement with ozonesonde climatologies from Antarctic stations (37) (*SI Appendix*, Fig. S5), mainly between 180 and 80 hPa.

The evolution of iodine-driven ozone loss over Antarctica between 1980 and 2015 shows a pronounced seasonal cycle that oscillates from the sunlit months to the winter, with peak ozone losses in the lowermost stratosphere (Fig. 2). Indeed, iodine chemistry reduces the background ozone abundance before, during, and after the ozone hole develops each year, although the dominant depletion channels during each period differ. Maximum absolute differences are observed during austral summer (December–February), whereas the maximum relative differences are modeled during October and November. The simulations also show that the highest iodine influence on ozone loss occurred at the beginning of the 1990s, after the eruption of Mount Pinatubo on June 15, 1991 (Fig. 2*A*). This was associated with the enhanced injection of sulfate aerosol particles to the stratosphere from the volcanic eruption, about two orders of magnitude higher than background levels (38, 39), and the subsequent increase in heterogeneous recycling of not only iodine but also bromine and chlorine reservoirs, on those substrates (reactions in *SI Appendix*, Table S4). The comparatively larger iodine impact in the post-Pinatubo years (*SI Appendix*, Fig. S6) implies the sensitivity of spring iodine ozone depletion to halogen recycling on stratospheric aerosols and interhalogen cycling with bromine and chlorine (see next section).

We now explore the iodine influence on the spatiotemporal development of the Antarctic ozone hole. In absolute terms, the effect of iodine on Antarctic stratospheric ozone loss in the 11- to 16-km altitude range is approximately constant during most of the summer, destroying ~37 ppbv (~6%) (Fig. 4*A* and *SI Appendix*, Fig. S7). During autumn and spring, the impact is ~31 ppbv (~5%) and ~38 ppbv (~11%), respectively. Iodine chemistry also influences the initial formation and closure stages of the ozone hole (Fig. 4*B*). The results show that considering iodine advances the beginning by about 5 d and delays the closure of the ozone hole (3 d to 5 d) (Fig. 4*B*). Note that the iodine simulation has a lower stratospheric ozone background, and therefore the total ozone column drops below the 220-Dobson unit (DU) threshold, which defines the ozone hole region earlier in the season. The delay in the closure is due to the ongoing ozone loss by photolysis of OIO, J(OIO), which is the dominant pathway for iodine-driven ozone loss during summer and fall (Fig. 5*E*). However, from June to September, the rates of both the J(OIO) and IO_ClO pathways are equivalent and contribute equally to ozone depletion, while, in October, the IO_ClO pathways begin to decline, and ozone depletion is driven mainly by the J(OIO) channel (Fig. 5 *E* and *F*). Therefore, ozone depletion by iodine during the formation of the ozone hole occurs through a pure iodine channel J(OIO) plus cross-reactions with chlorine. The ozone loss rates for the three halogen families increase at the same time during spring; however, from October to December, the only ozone loss channel that maintains its spring efficiency is that of J(OIO) (*SI Appendix*, Fig. S8). Iodine also affects the size of the ozone hole area, expanding its geographical extension by ~11% or 1.2 million km^2 (Fig. 6), mostly at the beginning of spring (Fig. 4). In addition to the timing and area, the inclusion of iodine also alters the ozone hole mass deficit (defined as the total amount of mass that is a deficit relative to the amount of mass present for a value of 220 DU [https://ozonewatch.gsfc.nasa.gov]), being ~20% lower than in the simulation without iodine.

The Relative Importance of Iodine Compared to Bromine and Chlorine

The contribution of iodine chemical cycles (IO_x^{loss} cycles; see definition of loss cycles in Table 2) to ozone loss rates peaks in September (2.0×10^4 molecules per $cm^3 \cdot s^{-1}$) and then decreases to an approximately constant value ($\sim 1 \times 10^4$ molecules per $cm^3 \cdot s^{-1}$) during the rest of the sunlit months (Fig. 5). The interhalogen crossed $ClO_xBrO_x^{loss}$ cycles follow a similar seasonality, although their spring rate (up to 4.4×10^5 molecules per $cm^3 \cdot s^{-1}$) is almost two orders of magnitude higher than in summer ($\sim 5.7 \times 10^3$ molecules per $cm^3 \cdot s^{-1}$). This is related to the seasonality of the heterogeneous reactivation of chlorine and bromine radicals on polar stratospheric clouds (PSCs), which drive and dominate most of the catalytic ozone destruction within the ozone hole (8). However, the IO_x^{loss} seasonal cycle is less pronounced than that of chlorine, indicating that iodine-driven ozone loss is not as sensitive to heterogeneous reactivation since iodine gas-phase photochemical cycling is faster than those of bromine and chlorine (17, 40). IO_x^{loss} is dominated by J(OIO), which, together with the IO_HO_2 and the IO_BrO channels, drives the background

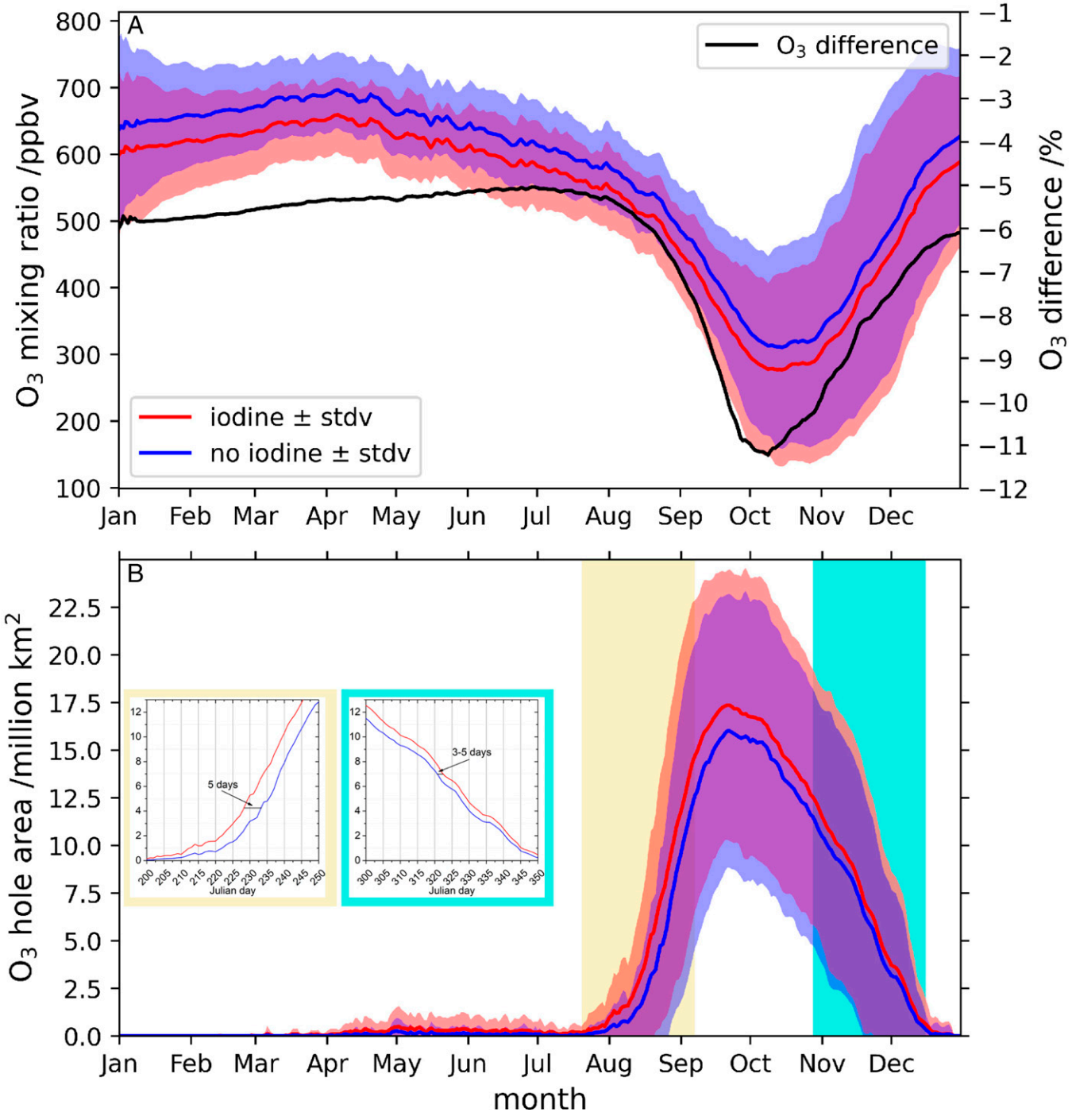

Fig. 4. Daily evolution of the ozone hole region during the 1980–2015 period. (*A*) Mean O_3 abundance at 11- to 16-km altitude in the region 90°S to 70°S for the simulation including the three halogens (red, "iodine"), and the simulation including only bromine and chlorine (blue, "no iodine"). Left *y* axis shows the averaged ozone mixing ratio, while right *y* axis corresponds to the difference (in percentage) between the "iodine" and "no iodine" runs. (*B*) Evolution of the ozone hole area, defined as the region of ozone values below 220 DU located south of 40°S (https://ozonewatch.gsfc.nasa.gov). Shaded areas represented the SD (±σ) in both ozone mixing ratio and ozone hole area.

ozone destruction by iodine in the stratosphere during the whole year. However, during spring, due to the reactivation of chlorine, the IO_ClO cycle increases strongly and even slightly exceeds the J(OIO) channel, enhancing ozone depletion by cross-reactions with chlorine (Fig. 5 *E* and *F* and *SI Appendix*, Fig. S8). For instance, this contribution to ozone depletion by cross-reactions with chlorine during spring is up to five percentage points in 2011, which represents approximately one-third of the iodine-driven ozone loss (*SI Appendix*, Fig. S9). During summer, when heterogeneous recycling does not occur, the channel IO_BrO is more important than the IO_ClO and equals the channel IO_HO_2, although all these channels are less efficient than the loss by OIO photolysis. During spring, the rates of the two main channels destroying ozone, (IO_ClO) and J(OIO), show the highest values at 11- to 16-km altitude in the 90°S to 70°S region (*SI Appendix*, Fig. S10), following the vertical distribution of IO, ClO, and OIO mixing ratios (*SI Appendix*, Fig. S11). Therefore, the impact of iodine on the

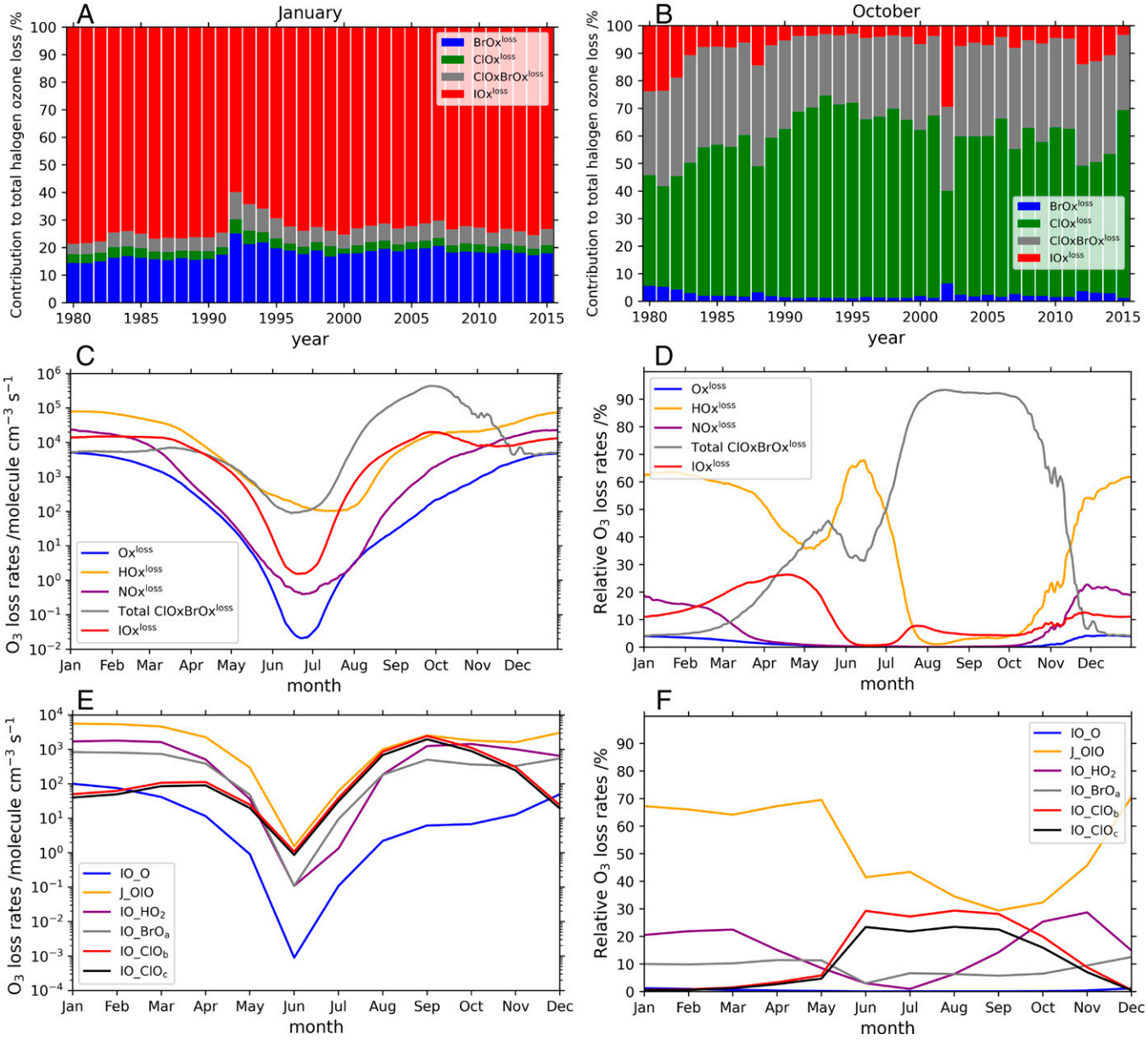

Fig. 5. Contribution of iodine chemistry to the evolution of the ozone hole, in terms of ozone loss rates, compared to chlorine and bromine and the rest of families (see definition of ozone loss rates in Table 2) at 11- to 16-km altitude and 90°S to 70°S latitude range. (*A* and *B*) The monthly averaged relative contribution of each halogen family with respect to total halogen ozone loss rate during the Antarctic summer (January) and spring (October) for the 1980–2015 period. (*C* and *D*) The daily ozone loss rates averaged during the 1980–2015 period in the same region. In *C* and *D*, the total $ClO_xBrO_x^{loss}$ term includes all contributions from chlorine and bromine to ozone loss (Total $ClO_xBrO_x = ClO_x^{loss} + BrO_x^{loss} + ClO_xBrO_x^{loss}$ according to ozone loss definitions in Table 2). (*E* and *F*) The averaged iodine absolute (*E*) and relative (*F*) ozone loss rates.

Antarctic ozone hole is strongest below 16 km (Fig. 2). Further analysis indicates that, before the ozone hole era (i.e., during 1970 when total Cl_y stratospheric mixing ratios were ∼60% smaller than in 2011), the contribution of IO_ClO cross-reactions during spring was ∼3 times smaller (*SI Appendix*, Fig. S12).

Chlorine activation from unreactive (e.g., $ClONO_2$ and HCl) to more photochemically reactive (e.g., Cl_2 and HOCl) species occurs on the surface of PSCs, during the Antarctic winter and spring (41, 42). Chlorine activation requires the presence of PSCs, and, therefore, its major contribution to ozone depletion is mainly restricted to springtime. However, the photoactivation of iodine chemistry occurs mainly in the gas phase; therefore, this lack of dependence upon the presence of PSCs results in efficient iodine-driven ozone loss during the entire sunlit period (Fig. 5) and both inside (90°S to 70°S) and outside (65°S to 55°S) the polar vortex (*SI Appendix*, Fig. S8). Our simulations show that IO_x^{loss} represents ∼73% of the halogen-driven ozone loss in summer (∼12% of the total ozone loss) and ∼8% in spring, at 11 to 16 km in the 90°S to 70°S region (Fig. 5 *A*, *B*, and *D*). Therefore, while iodine-mediated ozone destruction can be significant, although comparatively much smaller than that of ClO_xBrO_x cycles in spring, IO_x^{loss} dominates the halogen-driven ozone destruction chemistry in the Antarctic LS during summer (Fig. 5). This summertime destruction of ozone is driven both by J(OIO) and IO+HO_2 (which is largely natural) and by IO+BrO (which is dominated by anthropogenic contributions); see *SI Appendix*, Fig. S8.

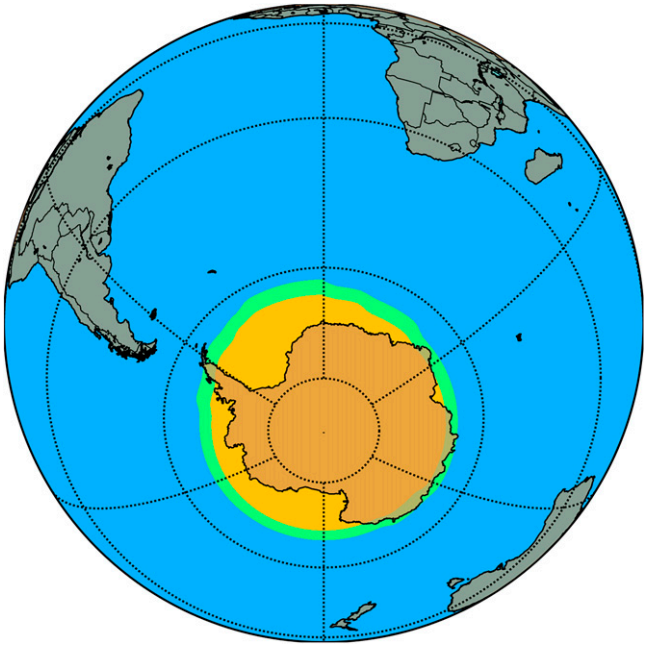

Fig. 6. Averaged ozone hole area (TOC < 220 DU) in the Antarctic spring (September and October) during the whole simulation period (1980–2015). The ozone hole area in the simulation without iodine is shown in yellow, while the expansion of the ozone hole area caused by iodine is depicted in green. The impact of iodine on the size of the ozone hole area is an expansion of ~11% or 1.2 million km^2.

In absolute terms, the most important ozone-depleting families are chlorine and bromine, although the abundance of each family is also very different (0.7, 13, and 1,335 pptv for I_y, Br_y, and Cl_y, respectively—see total inorganic bromine and chlorine definitions in *Materials and Methods*—at 16-km altitude in the 90°S to 70°S region). Thus, the ozone depletion efficacy of each family on a per atom basis can be estimated by normalizing the ozone loss rates of each family by their corresponding inorganic halogen abundance (i.e., I_y, Br_y, and Cl_y concentrations). *SI Appendix*, Fig. S13 shows that the family with highest ozone depletion efficacy is iodine, followed by bromine and with a much smaller value for chlorine.

The ozone loss caused by the currently estimated 5.0 ± 2.1 pptv of biogenic brominated VSLS that enter the stratosphere has been a subject of research in the last two decades (13–16, 43). Here we compare Antarctic lower stratospheric (90°S to 70°S at 11- to 16-km altitude) ozone loss driven by oceanic iodine emissions with that of biogenic bromine (*SI Appendix*, Fig. S7). During summer and fall, 0.77 pptv of iodine leads to a background ozone destruction of ~35 ppbv to 37 ppbv, while 5 ppt of biogenic bromine accounts for a background loss of ~30 ppbv to 45 ppbv. In spring, the ozone loss increases to 38 ppbv and 63 ppbv O_3 for iodine and biogenic bromine, respectively (*SI Appendix*, Fig. S7). We estimate that the ozone loss caused by 0.77 pptv of iodine in the Antarctic LS is equivalent to 3.1 pptv and 4.6 pptv of biogenic brominated VSLS in spring and the rest of the sunlit period, respectively.

The larger stratospheric ozone depletion efficacy of iodine, compared to equivalent amounts of bromine, highlights the potential importance that iodine chemistry can have under different halogen loading scenarios. In the future, the influence of anthropogenic long-lived ozone-depleting substances containing chlorine and bromine will decrease due to the Montreal Protocol, which, in turn, will increase the relative contribution of chlorinated and brominated VSLS (*SI Appendix*, Fig. S12) emitted from the oceans (13, 44). Ocean iodine emissions have tripled since 1950 (45–47), and it has been proposed that oceanic emissions of inorganic iodine may increase by ~20% following Representative Concentration Pathway 8.5 over the 2000–2100 period (30), although the increase in emissions would be much less under different scenarios. Consequently, the future relative contribution of iodine to stratospheric ozone loss may likely be higher than at present, with potential implications in delaying the future closing of the ozone hole, which warrant further investigation.

In summary, while we acknowledge existing uncertainties in iodine gas-to-particle partitioning and heterogeneous recycling of iodine reservoirs, as well as the need for observations of iodine in the Antarctic stratosphere, our results imply that the iodine contribution to chemical ozone destruction in the Antarctic ozone hole can potentially be significant, particularly in the lowermost stratosphere. Iodine chemistry destroys ozone in the Antarctic stratosphere through the J(OIO), IO_HO_2, and IO_BrO channels during the whole year, but also during spring due to the anthropogenic enhancement of Cl_y that increase the IO_ClO channels. Iodine atom–catalyzed ozone depletion has been neglected in the research of the Antarctic ozone hole since its discovery, due to the negligible amounts of iodine previously thought to enter the stratosphere (23). However, based on the recent quantification of stratospheric iodine injection (24, 25), our results suggest that iodine injection and chemistry need to be considered in models, along with chlorine and bromine, for fully accurate assessments and projections of halogen-mediated impacts on the background ozone abundances and ozone depletion in the Antarctic stratosphere.

Materials and Methods

WACCM REFC1SD Configuration. In this work, we have employed the Community Earth System Model, version 1 (CESM1), with the WACCM4 (26) as the atmospheric component. WACCM4 is a fully coupled state-of-the-art interactive chemistry climate model (48). The model setup is based on the REFC1SD (Chemistry-Climate Model Initiative [CCMI] past transient hindcast reference simulation in specified dynamics mode) configuration, including reanalysis for temperature and zonal and meridional winds, as well as surface pressure fields from the Modern Era Retrospective Analysis for Research and Applications (MERRA) (28, 49, 50). The standard WACCM4 chemical scheme includes the O_x, NO_x, HO_x, ClO_x, and BrO_x chemical families, along with gas-phase and heterogeneous reactions on liquid binary and ternary sulfate PSC particles, as well as solid nitric acid trihydrate and water ice polar stratospheric particles (51). The model (29) also incorporates an updated halogen chemistry scheme for halogens (chlorine, bromine, and iodine), as described in the following section.

Very Short-Lived Halogen Implementation in WACCM4. The benchmark WACCM4 troposphere–stratosphere–mesosphere–and–lower–thermosphere chemical scheme was updated to include previous developments of VSLS tropospheric halogen chemistry already implemented in the Community Atmosphere Model with Chemistry (CAM-Chem4) version of CESM1 (31, 32, 52). This includes the off-line emission of oceanic VSLS chlorocarbons, bromocarbons, and iodocarbons, the online computation of the sea salt aerosol (SSA) dehalogenation source due to the effective uptake of chloride and bromide from SSA, as well as the heterogeneous reactivation of inorganic halogen reservoirs on top of ice crystals in the UT (13, 31, 53). For the particular case of iodine chemistry, additional sources of inorganic iodine (in the form of HOI and I_2) due to the ozone-driven oxidation of aqueous iodide occurring at the ocean surface were also considered (30, 54–56). These additional sources of iodine are necessary to reconcile open ocean measurements of IO with current knowledge of iodine sources and chemistry (32). HOI and I_2 sources were implemented in CAM-Chem by Prados-Roman et al. (54) based on MacDonald et al. (55), and a follow-up study (57) confirmed that these sources are necessary to reproduce the IO measurements in the open marine boundary layer. Although the MacDonald et al. parameterization can be improved in some specific regions (58), the HOI and I_2 emission from CAM-Chem4 are also in agreement with the Goddard Earth Observing System model with atmospheric chemistry (GEOS-Chem) model (58). In this specified dynamics version of WACCM4, we employ MERRA reanalysis fields for temperature, winds, sea surface temperature, and surface pressure (50), which yield the inorganic

Table 2. Ozone loss rates definitions for the different families, including halogens (ClO_x, BrO_x, IO_x, and the crossed interhalogen cycles ClO_xBrO_x), O_x ($O+O_3$), HO_x ($H+OH+HO_2$), and NO_x ($NO+NO_2$)

Family	Reaction	Reaction name
ClOx	$ClO + O \rightarrow Cl + O_2$	ClO_O
	$Cl_2O_2 + hv \rightarrow 2\times Cl$	$J(Cl_2O_2)$
	$ClO + ClO \rightarrow 2\times Cl + O_2$	ClO_ClOa
	$ClO + ClO \rightarrow Cl_2 + O_2$	ClO_ClOb
	$ClO + HO_2 \rightarrow O_2 + HOCl$	ClO_HO_2
$ClOx^{loss} = 2 \times ClO\_O + 2 \times J(Cl_2O_2) + 2 \times ClO\_ClOa + 2 \times ClO\_ClOb + ClO\_HO_2$		
BrOx	$BrO + BrO \rightarrow 2\times Br + O_2$	BrO_BrO
	$BrO + O \rightarrow Br + O_2$	BrO_O
	$BrO + HO_2 \rightarrow HOBr + O_2$	BrO_HO_2
$BrOx^{loss} = 2 \times BrO\_BrO + 2 \times BrO\_O + BrO\_HO_2$		
ClOxBrOx	$BrO + ClO \rightarrow Br + Cl + O_2$	BrO_ClOb
	$BrO + ClO \rightarrow BrCl + O_2$	BrO_ClOc
$ClOxBrOx^{loss} = 2 \times BrO\_ClOb + 2 \times BrO\_ClOc$		
IOx	$IO + O \rightarrow I + O_2$	IO_O
	$OIO + hv \rightarrow I + O_2$	J(OIO)
	$IO + HO_2 \rightarrow HOI + O_2$	IO_HO_2
	$IO + BrO \rightarrow Br + I + O_2$	IO_BrOa
	$IO + ClO \rightarrow I + Cl + O_2$	IO_ClOb
	$IO + ClO \rightarrow ICl + O_2$	IO_ClOc
$IOx^{loss} = 2 \times IO\_O + 2 \times J(OIO) + IO\_HO_2 + 2 \times IO\_BrOa + 2 \times IO\_ClOb + 2 \times IO\_ClOc$		
Ox	$O + O_3 \rightarrow 2O_2$	O_O_3
	$O(^1D) + H_2O \rightarrow 2OH$	$O(^1D)\_H_2O$
$Ox^{loss} = 2 \times O\_O_3 + O(^1D)\_H_2O$		
HOx	$HO_2 + O \rightarrow OH + O_2$	HO_2_O
	$HO_2 + O_3 \rightarrow OH + 2*O_2$	$HO_2\_O_3$
	$OH + O \rightarrow H + O_2$	OH_O
	$OH + O_3 \rightarrow HO_2 + O_2$	OH_O_3
	$H + O_3 \rightarrow OH + O_2$	H_O_3
$HOx^{loss} = HO_2\_O + HO_2\_O_3 + OH\_O + OH\_O_3 + H\_O_3$		
NOx	$NO_2 + O \text{ -> } NO + O_2$	NO_2_O
	$NO_3 + hv \text{ -> } NO + O_2$	$J(NO_3)$
$NOx^{loss} = 2 \times NO_2\_O + 2 \times J(NO_3)$		

iodine emissions according to the observed meteorology from the 1980–2015 period. Note that this additional oceanic source of inorganic iodine is computed online based on modeled surface ozone and accounts for up to 60% of the current total inorganic iodine within the tropical tropopause layer (25), representing a significant contribution to the modeled stratospheric iodine injection. The model reproduces the only available direct measurement of stratospheric iodine injection (25). *SI Appendix*, Fig. S14 shows the vertical profile of I_y in the tropics and 60°S to 60°N regions in the present day (2015), including the uncertainties in those regions ($\pm\sigma$) and range of I_y in gas phase in the stratosphere. Regarding the chemical scheme, subsequent CAM-Chem updates mapping the heterogeneous recycling of $IONO_2$ and HOI on upper tropospheric ice crystals have also been included based in Saiz-Lopez et al. (24), which, in turn, considers the formation and photolysis of higher-order iodine oxides [$J\text{-}I_xO_y$ scheme; see Saiz-Lopez et al. (32)]. Table S2 in the supporting information of Saiz-Lopez et al. (24) compiles the individual inorganic iodine species that undergo washout and ice uptake within the model, as well as the specific parameterization and/or approximation used in each case.

Within the stratosphere, we mapped the standard scheme of heterogeneous recycling reactions for bromine and chlorine species (29, 59) to apply also for iodine (*SI Appendix*, Table S4). Even when the heterogeneous recycling of iodine species is expected to be faster than for the other halogens, and due to the scarcity of laboratory measurements (40), we mapped all reactive uptake coefficients (gammas) to those values from the equivalent brominated reactions (reactions in blue in *SI Appendix*, Table S4). However, and given the much larger photolytic efficiency of iodine species, the heterogeneous reactivation of iodine reservoirs represents only a minor contribution, and gas-phase photochemistry dominates iodine reactivation (17). In this regard, note that both CAM-Chem4 and WACCM4 include a logical condition based on the location of the local tropopause to allow for the stratospheric heterogeneous reactivation of halogen reservoirs on different types of aerosol surfaces, including sulfate, nitric acid trihydrate, and PSC substrates, whose surface area density (SAD) and effective radius are computed online (29). However, as WACCM includes a detailed treatment of stratosphere-to-troposphere exchange, these processes can result also in significant changes within the UT–LS composition. The definition of tropopause is based on the lapse rate (rate of decrease of temperature with height) (60).

Within the "iodine run" scheme, we assume that all the particulate iodine injected to the stratosphere is completely photolyzed back to gas-phase iodine due to the rapid enhancement of UV radiation in the upper stratosphere (*SI Appendix*, Fig. S3). This assumption is justified based on the particulate iodine speciation that shows that the dominant fraction of iodine in UT–LS is iodate (25), as well as on the experimental and theoretical determination of the iodate absorption spectra, that shows a maximum photodissociation efficiency within the 200- to 285-nm range (33, 34). The normalized enhancement in the photodissociation efficiency of particulate iodine (J-iodate, assuming all iodine in the aerosol is iodate) increases up to eight orders of magnitude between 10 and 40 km, highlighting the rapid reconversion of particulate iodate into gas-phase I_y.

Finally, in this work, we have also included a simulation including a parameterized representation of I_{part} by assuming that the rate of formation of I_{part} in the stratosphere is ~1% of the recycling rate of inorganic iodine reservoirs ($IONO_2$ and HOI) occurring on stratospheric aerosols (liquid binary and ternary sulfate PSC particles, solid nitric acid trihydrate, and water ice polar stratospheric particles) (reactions R15, R16, R31, R32, R47, and R48 in *SI Appendix*, Table S4). This particulate iodine formation is actually an uptake of reactive iodine on stratospheric aerosols, which, in turn, removes reactive iodine from the gas phase. In this I_{part} simulation, particulate iodine is not photolyzed back to the gas phase, thereby yielding a lower limit level of gas-phase iodine in the stratosphere. This simulation yields 0.07 ± 0.03 pptv IO in the LS in the nearly-current stratosphere (2010–2015), which reproduces the lower stratospheric IO measurements reported in Koenig et al. (25).

Model Runs. All model runs have been performed in SD mode (61), with dynamics specified from reanalysis (62) between 1980 and 2015. Four different configurations have been run as follows (Table 1): 1) the "iodine" run, from 1980 to 2015, includes updated iodine chemistry and emissions of both iodine (organic: CH_2I_2, CH_2IBr, CH_2ICl, CH_3I; inorganic: I_2 and HOI) and biogenic bromine ($CHBr_3$, CH_2Br_2, CH_2BrCl, $CHBr_2Cl$, and $CHBrCl_2$) VSLS; 2) the "no Br VSLS" run in which the emissions of biogenic bromine VSLS from the oceans are disabled, to account for the ozone depletion caused by these natural bromine species; 3) the "I_{part}" run, in which the conversion of gas-phase iodine to particulate iodine in the stratosphere is enabled—this case reproduces the gas-to-particle partitioning reported in Koenig et al. (25); and 4) the "no iodine" run, in which all iodine sources, both organic and inorganic, are disabled. Therefore, upper and lower limits of iodine influence on the ozone hole formation can be addressed by comparing the "iodine" vs. "no iodine" runs and "I_{part}" vs. "no iodine" runs, respectively, while the relative comparison between biogenic iodine and bromine to Antarctic stratospheric ozone depletion can be estimated from "iodine" vs. "no Br VSLS" cases. The sensitivity test "iodine run without the IO+BrO and IO+ClO channels" in the polar regions is a simulation equivalent to the iodine run, but zeroing the IO+ClO/BrO reactions (IO_BrOa, IO_ClOb, and IO_ClOc in Table 2) above the tropopause in the polar regions (90°S to 50°S and 50°N to 90°N) during 2011. The purpose of this experiment is to estimate the net effect of iodine in the ozone hole period, by means of the anthropogenically altered IO+ClO/BrO channels, compared to the "iodine" simulation. A second sensitivity has been performed making zero the values of the IO+ClO and IO+BrO cross-reaction channels above the tropopause during 2011, but also scaling chlorine and bromine levels to those in 1970. The purpose of this experiment is to show that the IO+ClO/BrO channels' sensitivity is impacted by the ClO_x/BrO_x abundance, and also to quantify the contribution from anthropogenic chlorine and bromine to those coupled reactions with iodine. The specified dynamics configuration employed in all runs ensures that the difference between simulations is only due to the inclusion of iodine, biogenic bromine VSLs, or the implementation of particulate iodine. Any other factor influencing Antarctic stratospheric ozone, like polar vortex descent (63) and/or PSC formation and sedimentation (29), is identical in all simulations and affects all runs in the same way. This is the WACCM4 state-of-the-art simulation employed in previous works on polar stratospheric ozone (29, 64). WACCM was configured with a horizontal resolution of 1.9° latitude by 2.5° longitude and 88 levels, from the surface to ~130 km, as in previous studies (29). The uncertainties of the iodine impact on the Antarctic stratospheric ozone are addressed by comparing the "I_{part}" (lower limit) and "iodine" (upper limit) runs. The uncertainties in the model output are represented in Fig. 4 and *SI Appendix*, Fig. S5 as the standard deviation STDV ($\pm\sigma$) in the ozone mixing ratio and ozone hole area throughout the 1980–2015 period.

Total inorganic bromine and chlorine definitions are as follows:

$$Br_y = Br + BrO + HOBr + BrONO_2 + HBr + BrCl + 2Br_2 + BrNO_2 + IBr$$

$$Cl_y = Cl + ClO + 2Cl_2 + 2Cl_2O_2 + OClO + HOCl + ClONO_2 + HCl + BrCl + ClNO_2 + ICl.$$

Data Availability. The software code for the CESM model is available from https://www.cesm.ucar.edu/models/.

All study data are included in the article and/or *SI Appendix*. Data related to this article are also available in Mendeley (https://data.mendeley.com/datasets/txcp862rp2/1).

ACKNOWLEDGMENTS. This study received funding from the European Research Council Executive Agency under the European Union's Horizon 2020 Research and Innovation Programme (Project ERC-2016-COG 726349 CLIMAHAL). D.E.K. is partly supported by NASA Grant 80NSSC19K0952. S.S. is partly supported by NSF-Atmospheric and Geospace Sciences Grant 1906719. The CESM project, which is supported primarily by the NSF, is led by the National Center for Atmospheric Research (NCAR), which is a major facility sponsored by the NSF under Cooperative Agreement 1852977. Computing resources, support, and data storage were provided by the Climate Simulation Laboratory at NCAR's Computational and Information Systems Laboratory, sponsored by the NSF. R.P.F thanks the Argentine Ministry of Science and the National Research Council for financial support (grants PICT 2019-02187 and SIIP M032/3853).

1. M. J. Molina, F. S. Rowland, Stratospheric sink for chlorofluoromethanes: Chlorine atom-catalysed destruction of ozone. *Nature* **249**, 810–812 (1974).
2. J. C. Farman, B. G. Gardiner, J. D. Shanklin, Large losses of total ozone in Antarctica reveal seasonal ClOx/NOx interaction. *Nature* **315**, 207–210 (1985).
3. R. S. Stolarski *et al.*, Nimbus 7 satellite measurements of the springtime Antarctic ozone decrease. *Nature* **322**, 808–811 (1986).
4. R. L. de Zafra *et al.*, High concentrations of chlorine monoxide at low altitudes in the Antarctic spring stratosphere: Diurnal variation. *Nature* **328**, 408–411 (1987).
5. C. B. Farmer, G. C. Toon, P. W. Schaper, J.-F. Blavier, L. L. Lowes, Stratospheric trace gases in the spring 1986 Antarctic atmosphere. *Nature* **329**, 126–130 (1987).
6. S. Solomon, G. H. Mount, R. W. Sanders, A. L. Schmeltekopf, Visible spectroscopy at McMurdo Station, Antarctica: 2. Observations of OClO. *J. Geophys. Res. Atmos.* **92**, 8329–8338 (1987).
7. J. G. Anderson, D. W. Toohey, W. H. Brune, Free radicals within the Antarctic vortex: The role of CFCs in Antarctic ozone loss. *Science* **251**, 39–46 (1991).
8. S. Solomon, Stratospheric ozone depletion: A review of concepts and history. *Rev. Geophys.* **37**, 275–316 (1999).
9. M. B. McElroy, R. J. Salawitch, S. C. Wofsy, J. A. Logan, Reductions of Antarctic ozone due to synergistic interactions of chlorine and bromine. *Nature* **321**, 759–762 (1986).
10. S. A. Montzka, J. H. Butler, B. D. Hall, D. J. Mondeel, J. W. Elkins, A decline in tropospheric organic bromine. *Geophys. Res. Lett.* **30**, 1826 (2003).
11. B.-M. Sinnhuber, N. Sheode, M. Sinnhuber, M. P. Chipperfield, W. Feng, The contribution of anthropogenic bromine emissions to past stratospheric ozone trends: A modelling study. *Atmos. Chem. Phys.* **9**, 2863–2871 (2009).
12. M. Dorf *et al.*, Long-term observations of stratospheric bromine reveal slow down in growth. *Geophys. Res. Lett.* **33**, L24803 (2006).
13. R. P. Fernandez, D. E. Kinnison, J. F. Lamarque, S. Tilmes, A. Saiz-Lopez, Impact of biogenic very short-lived bromine on the Antarctic ozone hole during the 21st century. *Atmos. Chem. Phys.* **17**, 1673–1688 (2017).
14. World Meteorological Organization. "Scientific assessment of ozone depletion: 2018" (Global Ozone Research and Monitoring Project Rep. 58, World Meteorological Organization, 2018).
15. P. A. Wales *et al.*, Stratospheric injection of brominated very short-lived substances: Aircraft observations in the Western Pacific and representation in global models. *J. Geophys. Res. Atmos.* **123**, 5690–5719 (2018).
16. R. J. Salawitch *et al.*, Sensitivity of ozone to bromine in the lower stratosphere. *Geophys. Res. Lett.* **32**, L05811 (2005).
17. S. Solomon, R. R. Garcia, A. R. Ravishankara, On the role of iodine in ozone depletion. *J. Geophys. Res. Atmos.* **99**, 20491–20499 (1994).
18. A. Butz *et al.*, Constraints on inorganic gaseous iodine in the tropical upper troposphere and stratosphere inferred from balloon-borne solar occultation observations. *Atmos. Chem. Phys.* **9**, 7229–7242 (2009).
19. G. Berthet, J.-B. Renard, M. Chartier, M. Pirre, C. Robert, Analysis of OBrO, IO, and OIO absorption signature in UV-visible spectra measured at night and at sunrise by stratospheric balloon-borne instruments. *J. Geophys. Res. Atmos.* **108**, 4161 (2003).
20. H. Bösch *et al.*, Upper limits of stratospheric IO and OIO inferred from center-to-limb-darkening-corrected balloon-borne solar occultation visible spectra: Implications for total gaseous iodine and stratospheric ozone. *J. Geophys. Res. Atmos.* **108**, 4455 (2003).
21. I. Pundt, J.-P. Pommereau, C. Phillips, E. Lateltin, Upper limit of iodine oxide in the lower stratosphere. *J. Atmos. Chem.* **30**, 173–185 (1998).
22. P. O. Wennberg, J. W. Brault, T. F. Hanisco, R. J. Salawitch, G. H. Mount, The atmospheric column abundance of IO: Implications for stratospheric ozone. *J. Geophys. Res. Atmos.* **102**, 8887–8898 (1997).
23. World Meteorological Organization, "Scientific Assessment of Ozone Depletion: 2014" (Global Ozone Research and Monitoring Project Rep. 55, World Meteorological Organization, 2014).
24. A. Saiz-Lopez *et al.*, Injection of iodine to the stratosphere. *Geophys. Res. Lett.* **42**, 6852–6859 (2015).
25. T. K. Koenig *et al.*, Quantitative detection of iodine in the stratosphere. *Proc. Natl. Acad. Sci. U.S.A.* **117**, 1860–1866 (2020).
26. R. B. Neale *et al.*, The mean climate of the Community Atmosphere Model (CAM4) in forced SST and fully coupled experiments. *J. Clim.* **26**, 5150–5168 (2013).
27. D. R. Marsh *et al.*, Climate change from 1850 to 2005 simulated in CESM1(WACCM). *J. Clim.* **26**, 7372–7391 (2013).
28. R. R. Garcia, A. K. Smith, D. E. Kinnison, Á. de la Cámara, D. J. Murphy, Modification of the gravity wave parameterization in the Whole Atmosphere Community Climate Model: Motivation and results. *J. Atmos. Sci.* **74**, 275–291 (2017).
29. S. Solomon, D. Kinnison, J. Bandoro, R. Garcia, Simulation of polar ozone depletion: An update. *J. Geophys. Res. Atmos.* **120**, 7958–7974 (2015).
30. F. Iglesias-Suarez *et al.*, Natural halogens buffer tropospheric ozone in a changing climate. *Nat. Clim. Chang.* **10**, 147–154 (2020).
31. R. P. Fernandez, R. J. Salawitch, D. E. Kinnison, J.-F. Lamarque, A. Saiz-Lopez, Bromine partitioning in the tropical tropopause layer: Implications for stratospheric injection. *Atmos. Chem. Phys.* **14**, 13391–13410 (2014).
32. A. Saiz-Lopez *et al.*, Iodine chemistry in the troposphere and its effect on ozone. *Atmos. Chem. Phys.* **14**, 13119–13143 (2014).
33. Ó. Gálvez, M. T. Baeza-Romero, M. Sanz, A. Saiz-Lopez, Photolysis of frozen iodate salts as a source of active iodine in the polar environment. *Atmos. Chem. Phys.* **16**, 12703–12713 (2016).
34. K. Kim *et al.*, Nitrite-induced activation of iodate into molecular iodine in frozen solution. *Environ. Sci. Technol.* **53**, 4892–4900 (2019).
35. R. W. Saunders, R. Kumar, S. M. MacDonald, J. M. C. Plane, Insights into the photochemical transformation of iodine in aqueous systems: Humic acid photosensitized reduction of iodate. *Environ. Sci. Technol.* **46**, 11854–11861 (2012).

36. J. C. Gómez Martín, S. H. Ashworth, A. S. Mahajan, J. M. C. Plane, Photochemistry of OIO: Laboratory study and atmospheric implications. *Geophys. Res. Lett.* **36**, L09802 (2009).
37. S. Tilmes *et al.*, Technical Note: Ozonesonde climatology between 1995 and 2011: Description, evaluation and applications. *Atmos. Chem. Phys.* **12**, 7475–7497 (2012).
38. M. J. Mills *et al.*, Global volcanic aerosol properties derived from emissions, 1990–2014, using CESM1(WACCM). *J. Geophys. Res. Atmos.* **121**, 2332–2348 (2016).
39. S. Solomon, R. W. Portmann, T. Sasaki, D. J. Hofmann, D. W. J. Thompson, Four decades of ozonesonde measurements over Antarctica. *J. Geophys. Res. Atmos.* **110**, D21311 (2005).
40. A. Saiz-Lopez *et al.*, Atmospheric chemistry of iodine. *Chem. Rev.* **112**, 1773–1804 (2012).
41. S. Solomon, R. R. Garcia, F. S. Rowland, D. J. Wuebbles, On the depletion of Antarctic ozone. *Nature* **321**, 755–758 (1986).
42. P. J. Crutzen, F. Arnold, Nitric acid cloud formation in the cold Antarctic stratosphere: A major cause for the springtime 'ozone hole.' *Nature* **324**, 651–655 (1986).
43. L. D. Oman *et al.*, The effect of representing bromine from VSLS on the simulation and evolution of Antarctic ozone. *Geophys. Res. Lett.* **43**, 9869–9876 (2016).
44. R. Hossaini *et al.*, Efficiency of short-lived halogens at influencing climate through depletion of stratospheric ozone. *Nat. Geosci.* **8**, 186–190 (2015).
45. C. A. Cuevas *et al.*, Rapid increase in atmospheric iodine levels in the North Atlantic since the mid-20th century. *Nat. Commun.* **9**, 1452 (2018).
46. M. Legrand *et al.*, Alpine ice evidence of a three-fold increase in atmospheric iodine deposition since 1950 in Europe due to increasing oceanic emissions. *Proc. Natl. Acad. Sci. U.S.A.* **115**, 12136–12141 (2018).
47. X. Zhao, X. Hou, W. Zhou, Atmospheric Iodine (^{127}I and ^{129}I) record in spruce tree rings in the Northeast Qinghai-Tibet Plateau. *Environ. Sci. Technol.* **53**, 8706–8714 (2019).
48. V. Eyring, T. G. Shepherd, D. W. Waugh, Eds., *SPARC CCMVal Report on the Evaluation of Chemistry-Climate Models* (SPARC Office, 2010).
49. R. Gelaro *et al.*, The Modern-Era Retrospective Analysis for Research and Applications, version 2 (MERRA-2). *J. Clim.* **30**, 5419–5454 (2017).
50. M. M. Rienecker *et al.*, MERRA: NASA's Modern-Era Retrospective Analysis for research and applications. *J. Clim.* **24**, 3624–3648 (2011).
51. Jet Propulsion Laboratory, "Chemical kinetics and photochemical data for use in atmospheric studies" (JPL Publ. 10-6, Jet Propulsion Laboratory, Pasadena, CA, 2011).
52. C. Ordóñez *et al.*, Bromine and iodine chemistry in a global chemistry-climate model: Description and evaluation of very short-lived oceanic sources. *Atmos. Chem. Phys.* **12**, 1423–1447 (2012).
53. J. A. Barrera *et al.*, Seasonal impact of biogenic very short-lived bromocarbons on lowermost stratospheric ozone between 60° N and 60° S during the 21st century. *Atmos. Chem. Phys.* **20**, 8083–8102 (2020).
54. C. Prados-Roman *et al.*, A negative feedback between anthropogenic ozone pollution and enhanced ocean emissions of iodine. *Atmos. Chem. Phys.* **15**, 2215–2224 (2015).
55. S. M. MacDonald *et al.*, A laboratory characterisation of inorganic iodine emissions from the sea surface: Dependence on oceanic variables and parameterisation for global modelling. *Atmos. Chem. Phys.* **14**, 5841–5852 (2014).
56. L. J. Carpenter *et al.*, Atmospheric iodine levels influenced by sea surface emissions of inorganic iodine. *Nat. Geosci.* **6**, 108–111 (2013).
57. C. Prados-Roman *et al.*, Iodine oxide in the global marine boundary layer. *Atmos. Chem. Phys.* **15**, 583–593 (2015).
58. S. Inamdar *et al.*, Estimation of reactive inorganic iodine fluxes in the Indian and Southern Ocean marine boundary layer. *Atmos. Chem. Phys.* **20**, 12093–12114 (2020).
59. D. E. Kinnison *et al.*, Sensitivity of chemical tracers to meteorological parameters in the MOZART-3 chemical transport model. *J. Geophys. Res. Atmos.* **112**, D20302 (2007).
60. T. Reichler, M. Dameris, R. Sausen, Determining the tropopause height from gridded data. *Geophys. Res. Lett.* **30**, D20302 (2003).
61. V. Eyring *et al.*, Overview of IGAC/SPARC Chemistry-Climate Model Initiative (CCMI) community simulations in support of upcoming ozone and climate assessments. *SPARC Newsl.* **40**, 48–66 (2013).
62. S. Tilmes *et al.*, Representation of the community earth system model (CESM1) CAM4-chem within the Chemistry-Climate Model Initiative (CCMI). *Geosci. Model Dev.* **9**, 1853–1890 (2016).
63. S. E. Strahan, A. R. Douglass, P. A. Newman, S. D. Steenrod, Inorganic chlorine variability in the Antarctic vortex and implications for ozone recovery. *J. Geophys. Res. Atmos.* **119**, 14–98,109 (2014).
64. K. A. Stone, S. Solomon, D. E. Kinnison, On the identification of ozone recovery. *Geophys. Res. Lett.* **45**, 5158–5165 (2018).